CrystEngComm

ROYAL SOCIETY OF CHEMISTRY

PAPER

View Article Online
View Journal | View Issue

Cite this: *CrystEngComm*, 2021, **23**, 7658

Reversed crystal growth of metal organic framework MIL-68(In)†

Kirsty McRoberts and Wuzong Zhou *

Received 19th August 2021,
Accepted 13th October 2021

DOI: 10.1039/d1ce01120k

rsc.li/crystengcomm

An investigation of the crystal growth of metal organic framework MIL-68(In) under solvothermal conditions revealed a non-classical reversed crystal growth mechanism *via* a route of nanorods – orientated aggregation into polycrystalline microrods – surface recrystallisation into a hexagonal shell – extension of recrystallisation from the surface to the core of the microrods. Terephthalic acid molecules which are adsorbed onto the surface of nanorods are believed to strengthen the inter-particle interaction, leading to an early stage aggregation of the monocrystalline nanorods.

Introduction

Classical crystal growth theory follows the Bravais–Friedel–Donnay–Harker (BFDH) law, with the building units (atoms, molecules or ions) deposited layer-by-layer onto a nucleus.[1–3] Since crystal growth rate is inversely proportional to inter-planar distance, the final morphology is normally dominated by faces with the largest inter-planar distances, as these have the slowest growth rates.[4] Therefore, a polyhedral morphology often reflects crystal symmetry. According to this growth path, the developed particles will show at least two characteristic features. Firstly, at any stage of growth, the particles must be single-crystals. Secondly, the particle size must increase with the growth time. This crystal growth route is referred to as an ideal growth route of free crystals. However, this theory cannot explain the formation of many novel crystal morphologies, such as hollow crystals, low dimensional crystals, spherulites, core–shell, dendritic crystals, *etc.*[5–11] In many real crystal growth processes, either in a natural environment or in laboratory conditions, various factors can affect crystal growth. One of them is early stage aggregation.

When nanocrystallites form in a synthetic system, they face a competition between two different processes: continuously growing as free crystals, and aggregation into largely disordered particles. In the latter, the growth environment for free crystals is disturbed. The most active sites for further crystal growth or recrystallisation are the surface of the particles, leading to a polyhedral single-crystalline shell. The recrystallisation then extends from the particle surface to its core. This phenomenon is the so-called 'Reversed Crystal Growth'. It was first reported in 2007 for the growth of zeolite analcime.[5] The crucial step of aggregation could even take place before formation of nanocrystallites. Precursor molecules may aggregate into large non-crystalline particles.[12] Till now, many types of crystals have been found to follow this growth route, including zeolite A,[12] metal oxides,[13–15] organic crystals,[16] and metal organic frameworks (MOFs).[17] In these synthetic systems, both inorganic and organic species were used as precursors or structure directing agents. The inter-particle interaction is strong and early stage aggregation is notably enhanced. The reversed crystal growth was also found in calcite crystals in naturally occurring travertine crust, as well as in biomimetic calcite using gelatin (type B), gum arabic and chitosan as structure directing agents.[18] The non-classical crystal growth route seems to be quite common.[19,20]

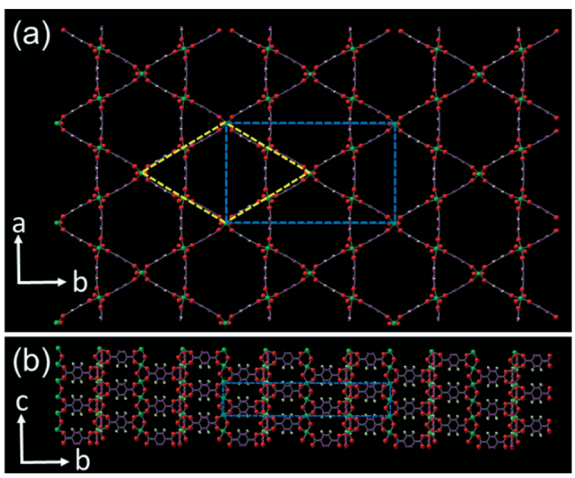

Fig. 1 Structural model of MIL-68(In) viewing down the (a) [001] and (b) [100] zone axes of the orthorhombic unit cell. In (a), the orthorhombic unit cell is drawn with blue dash lines and a pseudo-hexagonal unit cell is also shown in yellow dash lines.

EaStChem, School of Chemistry, University of St Andrews, Fife, KY16 9ST, UK. E-mail: wzhou@st-andrews.ac.uk

† Electronic supplementary information (ESI) available: More SEM images. See DOI: 10.1039/d1ce01120k

MOFs are formed by regular connection of inorganic clusters and organic molecules. Therefore, both inorganic and organic precursors must be used together. Strong interactions can be expected between precursors in the synthetic solution and in between small crystallites. In our previous work, we have found that cubic MOF-5 crystals were not developed from a single nucleus. Low density polycrystalline microcubes formed first, followed by surface-to-core recrystallisation into single crystals.[17] It is obvious that the morphology, crystallinity and porosity of MOF particles vary significantly with the growth time, and therefore their physico-chemical properties would also be expected to change.[21–24] MIL-68(In) is an interesting member of the MOF family, constructed by corner sharing indium–oxygen octahedra chains, connected with organic 1,4-benzenedicarboxylate (BDC) ligands. Its properties include 3D negative thermal expansion.[25] There are straight hexagonal channels surrounded by 6 trigonal channels parallel to the *c*-axis (Fig. 1). The structure of MIL-68(In) has an orthorhombic unit cell with the typical parameters a = 21.7739, b = 37.677, and c = 7.233 Å, space group *Cmcm* as reported previously.[26]

In the present work, crystal growth of MIL-68(In), with the composition of $In(OH)(O_2C–C_6H_4–CO_2)$ is investigated. A non-classical crystal growth mechanism is elucidated mainly based on electron microscopic results from specimens at different growth stages.

Results and discussion

MIL-68(In) specimens were solvothermally prepared *via* a reaction of indium nitrate and terephthalic acid in dimethylformamide (DMF) at 100 °C for a time between 1 h and 14 days. The powder X-ray diffraction (PXRD) patterns of the samples produced with different reaction times are shown in Fig. 2. All the patterns can be indexed to the orthorhombic unit cell of MIL-68(In). An increase in sharpness of the diffraction peaks, corresponding to an increase of the crystallinity, across the reaction times is observed. In particular, the intensity increase of the (220) peak is significant.

MOFs often form polymorphs. Two or more phases can be in a same sample or even in a same particle. As demonstrated by Islamoglu, *et al.*,[27] a secondary phase appeared at the centre of NU-1000 microrods. This normally takes place when the crystal growth is mainly controlled by a kinetical factor. A possible polymorph of MIL-68 is MIL-53, both containing the same components, but with different connection manners. MIL-68 presents triangular as well as hexagonal channels, while MIL-53 only has rhombic cavities.[28] They have different unit cells. In the present work, MIL-68 is the only phase observed in the XRD patterns in Fig. 2, and in scanning electron microscopy (SEM) images and selected area electron diffraction (SAED) patterns shown in Fig. 3.

The particle size and morphology of the produced MIL-68(In) crystals were observed from SEM images. The specimens with a long reaction time show a hexagonal microrod morphology (Fig. S1, ESI†), which is commonly observed. The reason to have a hexagonal morphology is that the *C*-centred orthorhombic unit cell can also be altered to a pseudo-hexagonal unit cell with a = 21.77 and c = 7.23 Å as demonstrated in Fig. 1a. The long axis of the microrods is parallel to the c axis. The side surface is terminated with the (110), (1$\bar{1}$0), (010), (0$\bar{1}$0), ($\bar{1}$10) and ($\bar{1}\bar{1}$0) planes of the orthorhombic unit cell, or the 6 equivalent {10$\bar{1}$0} planes of the pseudo-hexagonal unit cell. These facets are relatively stable without in-plane open bonds. To reveal whether these hexagonal microrods were developed from single nucleus, specimens at early stages were examined.

After 1 h reaction, the product contains short nanorods with a length of a few hundred nanometres and a width of dozens of nanometres. Most of these nanorods are separated in the specimen with some starting to aggregate (Fig. 3a). The crystalline structure of the nanorods was examined by SAED. Fig. 3b shows an SAED pattern from a nanorod (inset). It was found that the sample was electron beam sensitive and decomposed under the normal electron beam irradiation for high resolution transmission electron microscopy

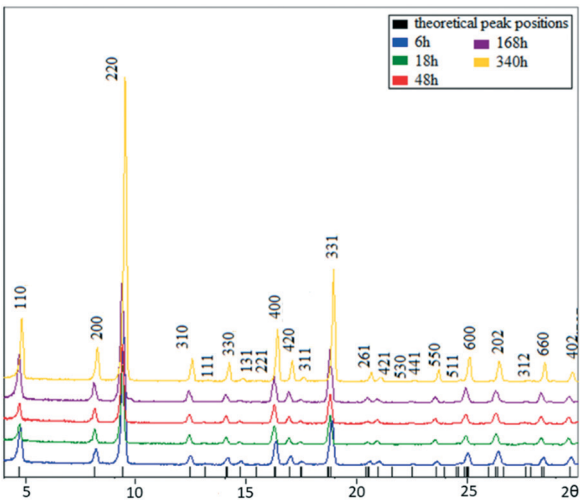

Fig. 2 PXRD patterns of MIL-68(In) from the samples with growth times of 6, 18, 48, 168, and 340 h. The top pattern from the 340 h sample is indexed to the orthorhombic unit cell.

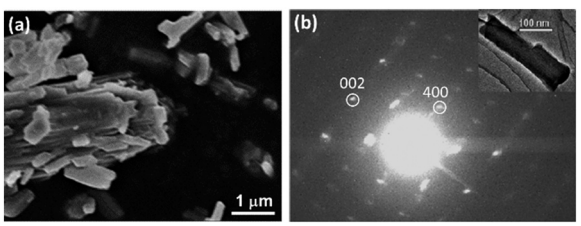

Fig. 3 (a) SEM image of the specimen after reaction for 1 h. (b) SAED pattern from a short nanorod (inset) of the 1 h sample, indexed to the orthorhombic unit cell.

(HRTEM) imaging within a few seconds. However, at a low magnification, TEM images and SAED patterns could be recorded with a low dose of electrons without notable specimen damage. The SAED pattern in Fig. 3b can be indexed to orthorhombic structure of MIL-68(In). It also indicates that nanorod is a single crystal and the long axis of the nanorod is along the [001] zone axis. Although a perfect hexagonal morphology did not appear yet in this sample, some flat facets of (010) and the equivalent planes formed. It is likely that the particles laid down on these facets. Therefore, the diffraction spots of (400) was often observed, since the direction of [100] was perpendicular to both the [010] and [001] directions of the orthorhombic unit cell. For the same reason, the (220) diffraction spots were rarely observed.

As seen in Fig. 1, the crystal structure of MIL-68(In) is constructed by chains of corner sharing InO_6 octahedrons along the *c* axis connected on the (*ab*) planes by the BDC ligands. The formation of nanorod morphology is understandable because the *d*-spacing of (002) planes is relative smaller in comparison with the *d*-spacings of (200) and (020) planes, leading to a faster growth rate along the *c* axis.

The process of nucleation and crystal growth to nanorods seem to be classical. However, increasing the reaction time, we did not observe further growth of individual particles. Instead, these nanorods aggregated into large microrods. Fig. 4a shows a microrod in the 3 h sample with a diameter of about 5 μm and about 15 μm in length. Fig. 4b shows a broken microrod, revealing a bunch of parallel nanorods. After reaction for 24 h, almost all the nanorods contributed to the construction of the microrods. We presume the excess terephthalic acid molecules adsorbed on the surface of the nanorods can act as bridges linking two nanorods using their two identical –COOH groups.

The side surface of the microrods had re-crystallised into single-crystal hexagonal shell as shown in Fig. 4c, while the inner part of the microrods were still polycrystalline. At the two ends, the positions of the nanorods were uneven. Therefore, single-crystal (001) planes did not form at this stage. The surface re-crystallisation into a single-crystalline shell is evidence of an important step of the so-called reversed crystal growth. A SAED pattern from this type of particle shows a single crystal-like pattern (Fig. 4d), indicating that the nanorods in the core of the particle are essentially well orientated. Some diffraction spots are diffused, meaning that the self-orientation of the nanorods is not perfect. The crystal direction along the long axis is still the [001] direction. Assuming the hexagonal particle lies down on a face, the observed $(400)_o$ diffraction spot indicates that the terminal faces of the particle must not be $\{100\}_o$, where the subscript "o" represents orthorhombic. Consequently, the 6 faces of the single-crystal shell should be $\{110\}_o$ of the orthorhombic unit cell or $\{100\}_h$ of the pseudo-hexagonal unit cell, where the subscript "h" represents hexagonal.

Aggregation of small particles is the key step of a reversed crystal growth. In growth of zeolite A, aggregation of precursor molecules forms non-crystalline spheres.[12] In the case of zeolite analcime, aggregation of crystalline nanoplates of 20 nm in size leads to disordered polycrystalline spheres.[5] The reversed crystal growth of RHO ZIF starts from aggregates of non-crystalline precursor molecules.[29] When crystals increase in size, the chance to aggregate becomes smaller. Therefore, it is unusual to see the self-orientated aggregation of nanorods of MIL-68 in the present work. A similar phenomenon has been observed in the formation of hematite nanotubes, where β-FeOOH nanorods aggregated in a parallel manner to form spindle-like particles.[30] However, these β-FeOOH nanorods were very thin, 5 nm in diameter. Self-orientated aggregation of such large nanorods (>50 nm in diameter and several micrometres in length) revealed in this work is rare and the inter-particle interaction must be strong. Since the terminal faces of the nanorods are likely $\{100\}_h$, which consist of chains of InO_6 octahedra linked by terephthalate dianions; a strong Coulomb force interaction can be expected between two facets of approaching particles.

Since the core of microrods is an aggregate of nanorods, the space between the nanorods would be filled by organic molecules and its density is lower than a single crystal. Fig. 5a shows a cross section of a microrod from 24 h sample prepared by using focused ion beam (FIB). Many holes can

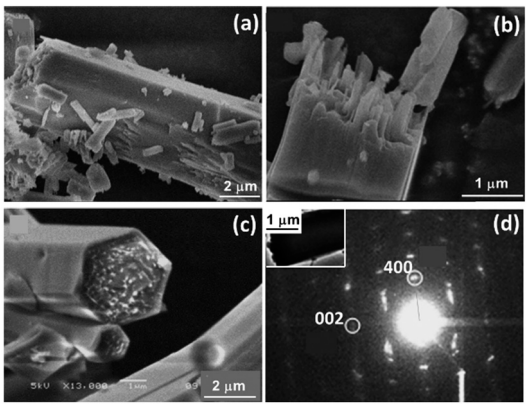

Fig. 4 (a) and (b) SEM images of 3 h sample. (c) SEM image of 24 h sample. (d) SAED pattern from a microrod (inset) of MIL-68 24 h sample.

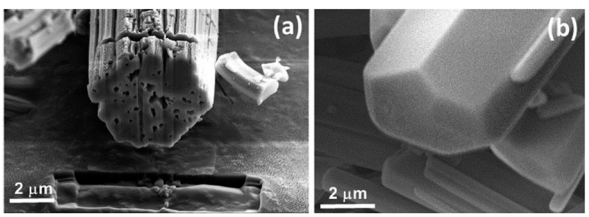

Fig. 5 SEM images of (a) the cross section of a microrod in the 24 h sample revealed by using FIB, and (b) an end of microrod from the 48 h sample.

be seen. With a further increase of reaction time, re-crystallisation extended from the surface to the core *via* an Ostwald ripening process. When the ends of microrods are not sealed, mass transportation from the solution to the cores is possible. Therefore, the density of the cores increases, rather than forming a large hole at the centre. In the 48 h sample, the ends of most microrods are sealed with a single-crystal layer and no holes are observed from images of cross sections, due to an increase of the density of MIL-68(In) crystals (Fig. 5b).

As the reaction progresses still further, the particle size did not change significantly. However, XRD patterns indicate that the crystallinity of the MIL-68(In) continuously increased up to 340 h (Fig. 2). That means the extension of re-crystallisation from the surface to the core took a significant time. Finally, all the hexagonal microrods became true single crystals.

To further confirm that the microrods at early stages were polycrystalline and organic molecules filled in the space between the nanorods, thermogravimetric analysis (TGA) of the 24 h sample (Fig. 6) was performed. It shows an initial percentage weight loss of 25%, followed by a second weight loss of 37%. The first weight loss is centred at 150 °C, corresponding to the loss of organic species from the sample. This may be due to organic species present at the surface of the nanorods or in the pores of the metal–organic framework. The second weight loss, occurring at 440 °C, is characteristic of the decomposition of the metal–organic framework from $In(OH)(O_2C–C_6H_4–CO_2)$ to indium oxide, carbon dioxide and water vapour.

In summary, although it is non-accidental that the final product of MIL-68(In) is hexagonal microrods, the crystal growth is non-classical, following the steps as shown in Fig. 7. Step 1, nucleation and growth of MIL-68(In) into nanorods occur. This process can be elucidated using the classical crystal growth theory. The long axis of the nanorods is parallel to the [001] zone axis of MIL-68(In), which is the direction of the fastest growth, corresponding to the smallest

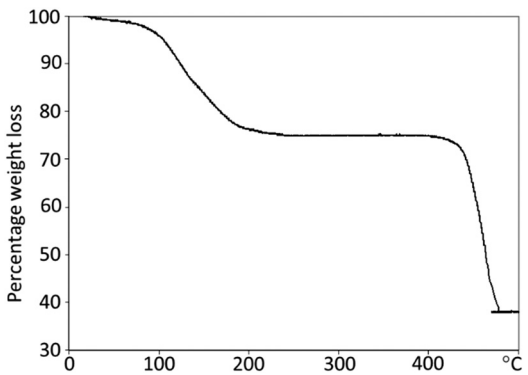

Fig. 6 Thermogravimetric analysis of 24 h sample of MIL-68(In), showing 25 and 37% weight loss at different temperatures, corresponding to loss of adsorbed organic species from the specimen, followed by the decomposition of MIL-68(In) to indium oxide, carbon dioxide, and water.

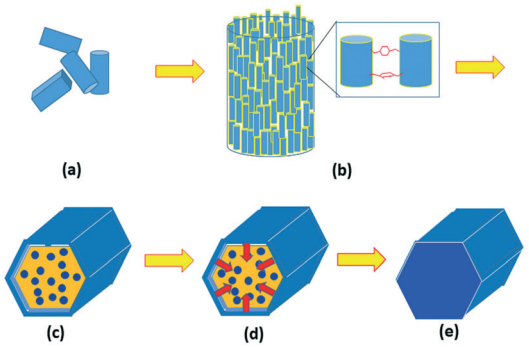

Fig. 7 Proposed formation mechanism of MIL-68(In) metal organic framework. (a) Step 1, nucleation and growth of nanorods of MIL-68(In). (b) Step 2, orientated aggregation of the nanorods into microrods. (c) Step 3, surface re-crystallisation into a single-crystal hexagonal shell with two ends unsealed, (d) step 4, extension of the re-crystallisation from the surface to the core. (e) Step 5, formation of single-crystal microrods.

d-spacing among the principal zone axes. Step 2, enhanced by the adsorbed organic molecules, the nanorods undergo an orientated aggregation into microrods. Step 3, surface re-crystallisation of the polycrystalline microrods takes place to form a single-crystal hexagonal shell, composed of six $\{100\}_h$ facets of the pseudo-hexagonal unit cell. Because the nanorods are uneven at the two ends of the microrods, single-crystal (001) planes do not form at the same time. Step 4, the re-crystallisation extends from the surface to the core *via* a further Ostwald ripening. On the other hand, the particle size does not increase significantly. Step 5, finally single-crystal microrods are achieved.

Experimental

MIL-68(In) was synthesized using an established method reported by Volkringer *et al.*[26] In a typical synthetic process, 1.32 mmol indium nitrate (99.9%, Aldrich) and 1.20 mmol terephthalic acid (98+%, Alfa Aesar) were combined with 5 ml dimethylformamide (DMF) (99%, Acros Organics) in a 30 ml autoclave. The sample was then placed in an oven for a solvothermal synthesis at 100 °C for a time between 1 h and 14 days. The reactions were stopped when they had reached the selected time frame, and new samples prepared. Post synthesis, the samples were filtered, washed with DMF, and oven dried at 60 °C overnight. Multiple samples from repeated syntheses were analysed to improve reliability.

The morphology and composition of the produced crystals were studied using a Jeol JSM-5600 scanning electron microscope operating at 20–30 kV and a Jeol JSM-6700F SEM operating at 1–5 kV. To reduce charging problem during SEM imaging, the samples were coated with a thin layer of gold. SAED patterns and transmission electron microscopic (TEM) images were obtained on a Jeol JEM-2011 electron microscope, operating at 200 kV. PXRD was carried out on a PANalytical Empyrean diffractometer using a Cu Kα X-ray source. TGA was performed using a Stanton Redcroft STA-780

series instrument at a heating rate of 5 °C per minute in a constant flow of air.

Conclusions

The growth mechanism of MIL-68(In) follows a reversed crystal growth route. Due to a strong inter-particle interaction, the MIL-68(In) nanorods aggregate in a parallel manner into large microrods. These polycrystalline microrods undergo surface recrystallisation into a single-crystal hexagonal shell. The recrystallisation then extends from the surface to the core of the particles. It is demonstrated that the formation of regular hexagonal morphology does not always mean the formation of a single crystal. The whole process of recrystallisation takes a long time due to large nanorods, much slower than reversed crystal growth in other zeolites and MOFs, in which the original core materials are either amorphous or very small nanocrystallites.

Conflicts of interest

Whilst this manuscript was being prepared, K. McR. left the University of St Andrews and now works for the RSC.

Acknowledgements

K. McR. wishes to thank University of St Andrews for a scholarship. She also wishes to thank Mr Ross Blackley for helping with the use of SEM and TEM microscopes and Mrs Sylvia Williamson for performing the TGA experiments.

References

1 A. Bravais, *Études Crystallographiques*, Gauthier-Villars, Paris, 1866.
2 M. G. Friedel, *Bull. Soc. Fr. Mineral.*, 1907, **30**, 326.
3 J. D. H. Donnay and D. Harker, *Am. Mineral.*, 1937, **22**, 446.
4 R. Docherty, G. Clydesdale, K. J. Roberts and P. Bennema, *J. Phys. D: Appl. Phys.*, 1991, **24**, 89.
5 X. Y. Chen, M. H. Qiao, S. H. Xie, K. N. Fan, W. Z. Zhou and H. Y. He, *J. Am. Chem. Soc.*, 2007, **129**, 13305.
6 H. F. Greer, M. Liu, C. Mou and W. Z. Zhou, *CrystEngComm*, 2016, **18**, 1585.
7 W.-H. Li, J. Q. Lv, Q. H. Li, J. F. Xie, N. K. Ogiwara, Y. Y. Huang, H. J. Jiang, H. Kitagawa, G. Xu and Y. B. Wang, *J. Mater. Chem. A*, 2019, **7**, 10431.
8 J. H. Jeong, H.-C. Woo and M. H. Kim, *RSC Adv.*, 2021, **11**, 22826.
9 W. Li, J. Yang, S. Du, E. Macaringue, Y. Wang, S. Wu and J. Gong, *Ind. Eng. Chem. Res.*, 2021, **60**, 6048.
10 J. Zhang, S. Bai, Z. Chen, Y. Wang, L. Dong, H. Zheng, F. Cui and M. Hong, *J. Mater. Chem. A*, 2017, **5**, 20757.
11 M. Pan, P. Li, J. Zheng, Y. Liu, Q. Kong, H. Tian and R. Li, *Mater. Chem. Phys.*, 2017, **194**, 49.
12 H. Greer, P. S. Wheatley, S. E. Ashbrook, R. E. Morris and W. Z. Zhou, *J. Am. Chem. Soc.*, 2009, **131**, 17986.
13 M. L. Moreira, J. Andres, V. R. Mastelaro, J. A. Varela and E. Longo, *CrystEngComm*, 2011, **13**, 5818.
14 H. Q. Zhan, X. F. Yang, C. M. Wang, J. Chen, Y. P. Wen, C. L. Liang, H. F. Greer, M. M. Wu and W. Z. Zhou, *Cryst. Growth Des.*, 2012, **12**, 1247.
15 B. Xu, B. B. Huang, H. F. Cheng, Z. Y. Wang, X. Y. Qin, X. Y. Zhang and Y. Dai, *Chem. Commun.*, 2012, **48**, 6529.
16 J. R. G. Sander, D.-K. Bučar, J. Baltrusaitis and L. R. MacGillivray, *J. Am. Chem. Soc.*, 2012, **134**, 6900.
17 C. M. Zheng, H. F. Greer, C.-Y. Chiang and W. Z. Zhou, *CrystEngComm*, 2014, **16**, 1064.
18 A. Ritchie, M. Watson, R. Turnbull, Z. Lu, M. Telfer, J. Gano, K. Self, H. F. Greer and W. Z. Zhou, *CrystEngComm*, 2013, **15**, 10266.
19 S. Tao, X. Li, H. Gong, Q. Jiang, W. Yu, H. Ma, R. Xu and Z. Tian, *Microporous Mesoporous Mater.*, 2018, **262**, 182.
20 T. Zheng, C. Wang, C. Xu and Q. Hu, *Mater. Lett.*, 2020, **263**, 127274.
21 Z.-Y. Gu, J.-Q. Jiang and X.-P. Yan, *Anal. Chem.*, 2011, **83**, 5093.
22 Y. Liu, Z. Ng, E. A. Khan, H.-K. Jeong, C.-B. Ching and Z. Lai, *Microporous Mesoporous Mater.*, 2009, **118**, 296.
23 N. Stock and S. Biswas, *Chem. Rev.*, 2012, **112**, 933.
24 U. Mueller, M. Schubert, F. Teich, H. Puetter, K. Schierle-Arndt and J. Pastré, *J. Mater. Chem.*, 2006, **16**, 626.
25 Z. N. Liu, Q. Li, H. Zhu, K. Lin, J. X. Deng, J. Chen and X. R. Xing, *Chem. Commun.*, 2018, **54**, 5712.
26 C. Volkringer, M. Meddouri, T. Loiseau, N. Guillou, J. Marrot, G. Férey, M. Haouas, F. Taulelle, N. Audebrand and M. Latroche, *Inorg. Chem.*, 2008, **47**, 11892.
27 T. Islamoglu, K. Otake, P. Li, C. T. Buru, A. W. Peters, I. Akpinar, S. J. Garibay and O. K. Farha, *CrystEngComm*, 2018, **20**, 5913.
28 A. Fateeva, P. Horcajada, T. Devic, C. Serre, J. Marrot, J.-M. Grenèche, M. Morcrette, J.-M. Tarascon, G. Maurin and G. Férey, *Eur. J. Inorg. Chem.*, 2010, 3789.
29 K. Self, M. Telfer, H. F. Greer and W. Z. Zhou, *Chem. – Eur. J.*, 2015, **21**, 19090.
30 J. L. Chen, S. Macfarlane, C. X. Zhang, K. Yu and W. Z. Zhou, *Cryst. Growth Des.*, 2017, **17**, 5975.

